Soft Matter

www.rsc.org/softmatter

Volume 8 | Number 48 | 28 December 2012 | Pages 11951–12146

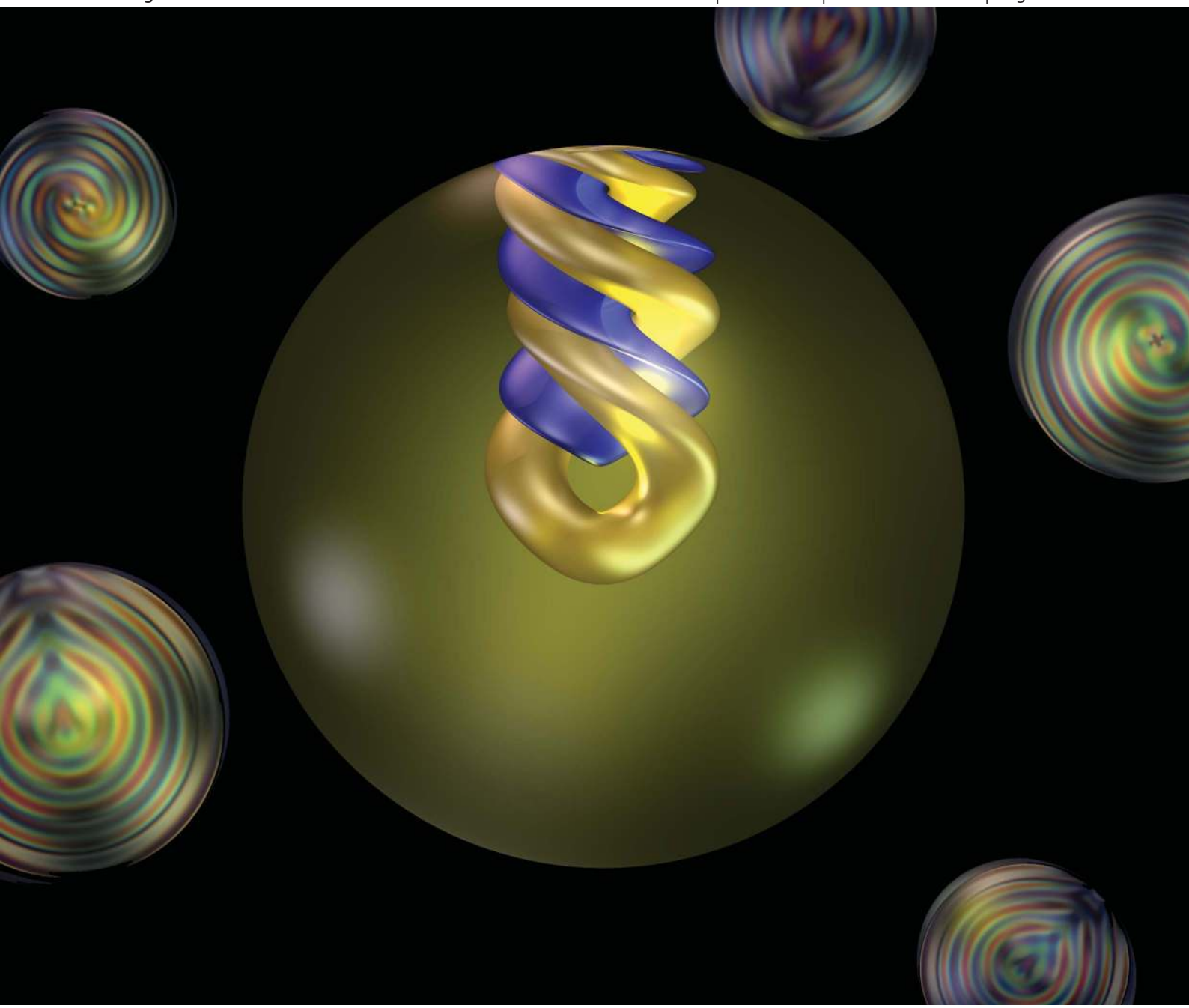

ISSN 1744-683X

RSC Publishing

PAPER

David Seč *et al.*

Geometrical frustration of chiral ordering in cholesteric droplets

1744-683X(2012)8:48;1-0

Soft Matter

Dynamic Article Links

Cite this: *Soft Matter*, 2012, **8**, 11982

www.rsc.org/softmatter

PAPER

Geometrical frustration of chiral ordering in cholesteric droplets

David Seč,*[a] Tine Porenta,[a] Miha Ravnik[ab] and Slobodan Žumer[abc]

Received 4th September 2012, Accepted 3rd October 2012
DOI: 10.1039/c2sm27048j

Frustration of chiral ordering is explored in cholesteric liquid crystal droplets with planar degenerate anchoring using numerical modeling. Droplets of variable pitches are studied, demonstrating the role of a gradually increasing cholesteric pitch and the corresponding equilibrium structures. All previously known structures are identified but with notable differences. The structures presented with director fields are complemented with a detailed description of the defect regions. The characteristic half-diameter +2 disclination from previous studies is found to be in fact a *double-helix* of two λ^{+1} disclination lines, whereas the full-diameter +1 disclination is composed of an alternating series of $\tau^{-1/2}$ and $\lambda^{+1/2}$ disclination rings. Finally, two new meta-stable cholesteric structures -Lyre and Yeti- are found, which are characterised by complex compositions of cholesteric disclinations.

1 Introduction

Frustration by chirality in liquid crystals is emerging as a route towards novel soft matter optical structures for use in advanced optics and photonics.[1,2] Complex toron structures were stabilised in cholesteric liquid crystals by using modulated Laguerre–Gaussian laser beams.[3] Continuous rotation of cholesteric droplets was achieved by linearly polarized laser beams,[4,5] offering routes to rheological studies. Chiral liquid crystals were employed as Bragg resonators for micro-lasers with random or band-edge lasing,[1,2,6,7,15] where intrinsic chirality in cholesteric liquid crystals causes periodic helical twisting of the cholesteric molecular orientational order – effectively, the optical axis – which in turn acts as an optical resonator. The periodic modulation of the refractive index is closely related to the cholesteric pitch, which can be controlled by temperature,[8,9] chiral dopants,[10] optical illumination,[11] or even geometrical frustration.[13] Cholesteric liquid crystals with controllable pitch also appear in biological systems like short fragment DNA.[14] Indeed, advanced light characteristics can be achieved in cholesteric-based lasers, like "white" lasers in cholesteric cells,[2] and three-dimensional omnidirectional microlasers in cholesteric droplets.[1]

Cholesteric liquid crystals favour twisting of their average orientation – the nematic director – in planes. If the cholesteric is frustrated, when being enclosed into droplets, disclinations can form. The disclinations in cholesterics can be singular or non-singular in the nematic director field – the classification we use in this paper – but may have further topological or non-topological characteristics if also considering biaxiality and secondary directors.[16] The disclinations in cholesterics are usually distinguished into three classes[12,17,33] as represented in Fig. 1: $\lambda^{\pm m}$, $\tau^{\pm m}$, and $\chi^{\pm m}$. Note, that except for χ^{+1}, there is no twist of the nematic director along the disclination. Half-integer and integer m characterize their winding number. Fig. 1 shows examples of χ-screw disclinations. Note that χ-edge disclinations can also emerge in cholesterics.[13] Cholesteric disclination lines were largely explored in cholesteric cells.[18,19] Here, we show that they generically form in cholesteric droplets.

Three structures are found in cholesteric droplets with planar degenerate anchoring:[20–23] (i) radial spherical structure (RSS), (ii)

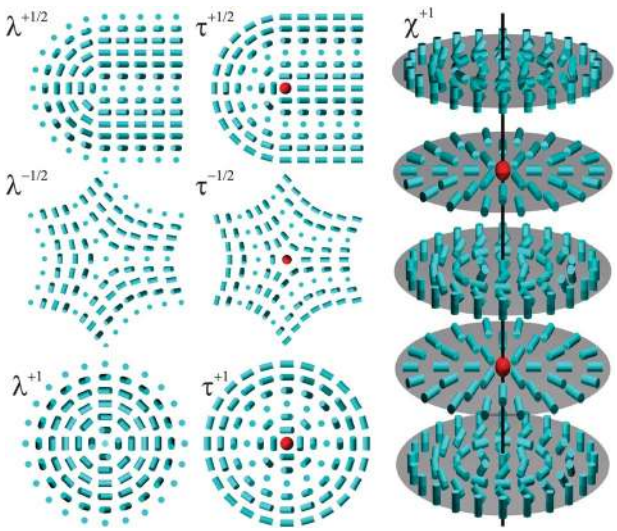

Fig. 1 Schematic representation of cholesteric disclination lines λ^m, τ^m and χ^m with various winding numbers m. The director is shown with blue cylinders while red spheres characterize regions with lower order parameters. The core of the χ disclination is drawn as a black line. Note that the λ^{+1}, τ^{+1}, and χ^{+1} disclinations can be energetically unstable.

[a]*Faculty of Mathematics and Physics, University of Ljubljana, 1000 Ljubljana, Slovenia.*
E-mail: david.sec@fmf.uni-lj.si
[b]*Center of Excellence NAMASTE, Jamova 39, 1000 Ljubljana, Slovenia*
[c]*Jožef Stefan Institute, Jamova 39, 1000 Ljubljana, Slovenia*

diametrical spherical structure (DSS), and (iii) planar bipolar structure (PBS). In experiments, most commonly the radial spherical structure is observed,[24] also known as the *spherulitic texture* or the *Frank-Pryce model*.[25] For low chirality and generally smaller droplets, the twisted bipolar director structure becomes energetically more favorable than the PBS structure.[21] In the radial spherical structure, the predicted +2 disclination shows an interesting analogy to the Dirac monopoles.[26] Finally, it is important to note that all current theoretical studies of cholesteric droplets were performed with director-based approaches, which covered only approximately the inherently present defect regions in the droplets that are elementarily important for optical applications. Here, we show that the defects are much more intricate and we explain their detailed structures.

In our study, we explore the cholesteric liquid crystal droplets with degenerate planar anchoring by using numerical Landau-de Gennes modeling. Two new structures and known structures are observed and fully analysed. We find the commonly expected +2 defect line in the radial spherical structure to be unstable, and we make a detailed view of its decomposition into a double-helix of two λ^{+1} defect lines. Also, the expected +1 defect line in the diametrical spherical structure is found to be unstable, and it evolves into a series of either $\lambda^{+1/2}$ and $\lambda^{-1/2}$ or $\lambda^{+1/2}$ and $\tau^{-1/2}$ rings. The stability of all six structures is explored, as dependent on the droplet size and the intrinsic material pitch.

2 Model and methods

A continuum mean field Landau-de Gennes (LdG) free energy approach is employed to model the chiral liquid crystal ordering in the cholesteric droplets. The tensorial order parameter Q_{ij} is used to construct the total free energy F, which is able to fully characterize the defect regions also. The central interest of this study is the effect of chirality; therefore, we use one elastic constant approximation. The following LdG free energy F is taken:[27,28]

$$F = \int_{\mathrm{LC}} \left\{ \frac{A}{2} Q_{ij} Q_{ji} + \frac{B}{3} Q_{ij} Q_{jk} Q_{ki} + \frac{C}{4} \left(Q_{ij} Q_{ji} \right)^2 \right\} \mathrm{d}V + \int_{\mathrm{LC}} \left\{ \frac{L}{2} \frac{\partial Q_{ij}}{\partial x_k} \frac{\partial Q_{ij}}{\partial x_k} + 2 q_0 L \varepsilon_{ikl} Q_{ij} \frac{\partial Q_{lj}}{\partial x_k} \right\} \mathrm{d}V + \int_S \left\{ \frac{W}{2} \left(\tilde{Q}_{ij} - \tilde{Q}_{ij}^{\perp} \right)^2 \right\} \mathrm{d}S, \quad (1)$$

where LC denotes the integration over the bulk of the liquid crystal (LC) and S over the surface of the droplet. The first term accounts for the variation of the nematic degree of order, *i.e.* the possible formation of singular defects; A, B, and C are material parameters. The second term penalises elastic distortions from the twisted cholesteric state with a single uniform helical axis, characterised by the pitch p_0. L is the elastic constant and $q_0 = 2\pi/p_0$ is the inverse pitch. As a measure of the relative size of the droplet with respect to the chiral pitch, it is useful to present the pitch in units of the droplet diameter as $p_0 = 4R/N$, where effectively, N corresponds to the number of π turns the director would make in a non-confined cholesteric along the distance equal to the droplet diameter $2R$. The final term accounts for the LC interaction with the *planar degenerate* surface, where W is the anchoring strength and $\tilde{Q}_{ij}^{\perp}$ and $\tilde{Q}_{ij}$ are related to the full order parameter tensor as defined by Fournier and Galatola.[28]

We minimize the total free energy F numerically by using an explicit Euler relaxation finite difference scheme on a cubic mesh.[29] The surface of the droplet is modeled as a spherical shell of mesh points with thickness equal to the mesh resolution. To cover the cholesteric twisting of the director and in particular the defects, typically more than 70 mesh points per pitch are used. For the director field Ansatze of the RSS and DSS structures, the approximate solutions from Bezić and Žumer[22] are used that in spherical coordinates read as:

$$\boldsymbol{n}(r,\Phi,\theta) = \cos\Omega \boldsymbol{e}_{\mathrm{r}} + \sin\Omega \boldsymbol{e}_{\phi} \text{ with } \Omega = (m-1)\Phi + q_0 z, \quad (2)$$

where m is the winding number of the disclination line (*i.e.* $m = 2$ for RSS and $m = 1$ for DSS), $\boldsymbol{e}_{\mathrm{r}}$ and $\boldsymbol{e}_{\phi}$ are unit vectors in spherical coordinates (r, θ, Φ) and z is the coordinate along the symmetry axis of the structures in Cartesian coordinates. For the PBS structure the initial conditions were chosen as in the undistorted cholesteric with layer normals in the y direction.

Symmetry and topological considerations suggest that further (novel) structures might form in the cholesteric droplets, and to access them numerically the Ansatze are constructed, based on the model of the dissociated χ^{+1} line in cholesterics.[13] The central cylindrical region of the droplet for $\rho < R_0$ (along the z axis; typically $R_0 \sim R/2$) is essentially a double twist cylinder of variable radius with respect to the coordinate z. Thus, in cylindrical coordinates and Cartesian basis, the director reads:

$$\boldsymbol{n}(\rho,\phi,z) = \left\{ -\sin(\phi)\sin\left(\frac{\omega\rho}{R_0}\right), \cos(\phi)\sin\left(\frac{\omega\rho}{R_0}\right), -\cos(\phi)\cos\left(\frac{\omega\rho}{R_0}\right) \right\}. \quad (3)$$

The director in the outer region ($\rho > R_0$) is taken as rotating cholesteric layers and reads:

$$\boldsymbol{n}(\rho,\Phi,z) = \{\sin(\Phi + \Psi), \cos(\Phi + \Psi), 0\}, \quad (4)$$

where $\psi = N\pi z/(2R)$ and $\omega = \pi + \frac{\pi}{2}\cos(\psi)$.

To examine the defect lines (either structure or possible escape in third dimension) a splay-bend parameter is extracted from the order parameter tensor field. The scalar splay-bend parameter S_{SB} determines the amount of the splay and bend deformations as a sum of the second derivatives of the order parameter tensor Q_{ij}:[30]

$$S_{\mathrm{SB}} = \frac{\partial^2 Q_{ij}}{\partial x_i \partial x_j}. \quad (5)$$

Note that S_{SB} is calculated in the units of nematic correlation length squared $\xi^2 \sim 44\ \mathrm{nm}^2$. The spatial distribution of the splay-bend parameter can determine disclination lines in the nematic director, both singular and non-singular. For the complete presentation of a singular defect line, the defect core should be shown additionally as an isosurface with a decreased scalar order parameter.

Polarization micrographs of cholesteric droplets are calculated with the Jones 2 × 2 matrix formalism. This formalism

incorporates the locally variable birefringence of the nematic refractive index – typically the leading contribution – but neglects reflections and refractions on the droplet surface.[31] More specifically, in this formalism, the light beam is propagated along a chosen direction and the total phase shift between ordinary and extraordinary polarisations is accumulated. We repeat the calculation for 10 different wavelengths in the approximate radiation spectra of the black body at 6000 K (*i.e.* the white light approximation). The results for each wavelength are then summed with weights of the RGB color spectra to form color images that reproduce experimental observations. The polarization micrographs are calculated for the director structure scaled by a factor of 3 to the size of typical experiments[32] for a more quantitative comparison.

Material parameters of a typical cholesteric liquid crystal are used. If not stated differently, the following numerical values are used: $L = 4 \times 10^{-11}$ N, $A = -0.172 \times 10^6$ J m^{-3}, $B = -2.12 \times 10^6$ J m^{-3}, $C = 1.73 \times 10^6$ J m^{-3}, $W = 1 \times 10^{-3}$ J m^{-2}, and for polarization micrographs $n_o = 1.5$ and $n_e = 1.7$ are used as ordinary and extraordinary indices of refraction, respectively.

3 Structures in cholesteric droplets

Six (meta)stable orientational profiles are found in cholesteric droplets with planar degenerate anchoring, each characterised by its specific configuration of the director profile and the topological defects: (i) the diametrical spherical structure (DSS), (ii) the radial spherical structure (RSS), (iii) the bipolar structure (BS), (iv) the planar bipolar structure (PBS), (v) the Lyre structure, and (vi) the Yeti structure. The structures differ in the number and position of the defects, the symmetry of the director field, and the stability regimes. We should comment that the earlier known structures, which are presented in the literature[21–23] (the DSS, RSS, PBS) agree in general features with the presented structures, but there are substantial differences in the defect regions. Two structures that we found were to the best of our knowledge not predicted or observed before – the Lyre, and Yeti structures.

3.1 Diametrical spherical structure

The diametrical spherical structure (DSS, Fig. 2a) is the most symmetric structure in cholesteric droplets with degenerate planar surface anchoring. It exhibits cylindrical symmetry with the symmetry axis along the z direction, *i.e.* through the centers of the ring defects (in red, Fig. 2a). The director field forms curved cholesteric layers with the layer normals in the radial direction (except along the $+z$ and $-z$ direction). The field is visualized as a series of concentrically positioned tori of deformed double twist cylinders (the cross-section of the deformed cylinder being rather banana shaped instead of circular). The central torus is constructed from a double twist cylinder and resembles the triple-twist toron structures stabilized by Smalyukh *et al.*[3] Along the z axis, a series of bulk ring defects emerge to compensate for the director field imposed by the tori. Interestingly, we always find an even number of the defect rings regardless of the cholesteric pitch. More specifically, their number is found to depend on the ratio of the droplet radius *versus* the cholesteric pitch and is equal to $N_{def} = 2\lfloor (N-2)/2 \rfloor$ when the structure is stable, and $N_{def}^{meta} = 2\lfloor N/2 \rfloor$ when structure is meta-stable (typically only for N not being even), where $\lfloor\rfloor$ represents the integral part of a number. In addition to the bulk defect rings, two surface boojum defects emerge, positioned diametrically opposite on the z axis. The series of observed bulk defect rings and surface boojums is similar to the previously predicted[22] diametrical +1 disclination line; however, our more detailed study shows that actually a χ^{+1} disclination line evolves into energetically favorable alternating rings of $\tau^{-1/2}$ and $\lambda^{+1/2}$ lines with the director roughly homogeneous along the z direction inside the effective region encompassed by these rings. Note how the cross-section of the escaped center of the line alternates from circular to radial +1 configuration. We should stress that the director rotates only by $\pi/2$ in the z direction between the two lines. Such a structure is therefore essentially different from the dissociated model[13,34] of the χ^{+1} line in cholesteric where the line decomposes into non-singular $\lambda^{+1/2}$ and $\lambda^{-1/2}$ lines and the director rotates for π between the lines. The dissociated model is later shown to lead to Lyre and Yeti structures (Fig. 5).

3.2 The radial spherical structure

The radial spherical structure (RSS, Fig. 2b) is most commonly observed in experiments[24] and effectively consists of distorted double twist tori with a variable (angle dependent) minor radii. In comparison to the diametrical spherical structure, the symmetry of double twist tori having homogeneous minor radius is broken and effectively one side of the torus expands over the other side. There are no *singular* bulk defects in the nematic director in the RSS structure; however, to account for the contact regions between the double twist tori, cholesteric λ disclinations emerge along a distinct direction from the center of the droplet to the surface – the structure is monopolar. The escaped disclinations are found to be a *double helix* of two cholesteric λ^{+1} disclination lines, as visualized in Fig. 2b in yellow with a negative splay-bend parameter.[30] Contrary to the diametrical spherical structure (DSS), here, the cross-section of both line defects is always circular and the lines rotate around the axis going through the center of the droplet. At the surface of the droplet, each line ends with a singular surface boojum defect. In contrast, in the center of the droplet the two λ^{+1} lines of the double helix fuse. Alternatively, this double helix cholesteric defect structure can be interpreted as a line starting at one of the surface defects, then winding towards the center of the droplet, until it returns winding around itself back to the other surface defect. Interestingly, we find that the handedness of local twist in the two λ^{+1} disclination lines is opposite to the handedness of the full double helix. Clearly, this structure is not rotationally symmetric around this defect direction (z axis), which indeed is seen in experiments.[36]

The calculated double-helix defect structure in the radial spherical structure – which relates to the distinct wrapping of cholesteric layers – is notably different from the currently predicted structure of the non-singular disclination line with winding number +2 in the Frank-Pryce model.[25] A more detailed comparison is shown in Fig. 3. In order to show the direct difference between our calculated and Frank-Pryce structure, the director fields in defect regions of both structures are reproduced by analytically constructing the characteristic director fields:[13,17]

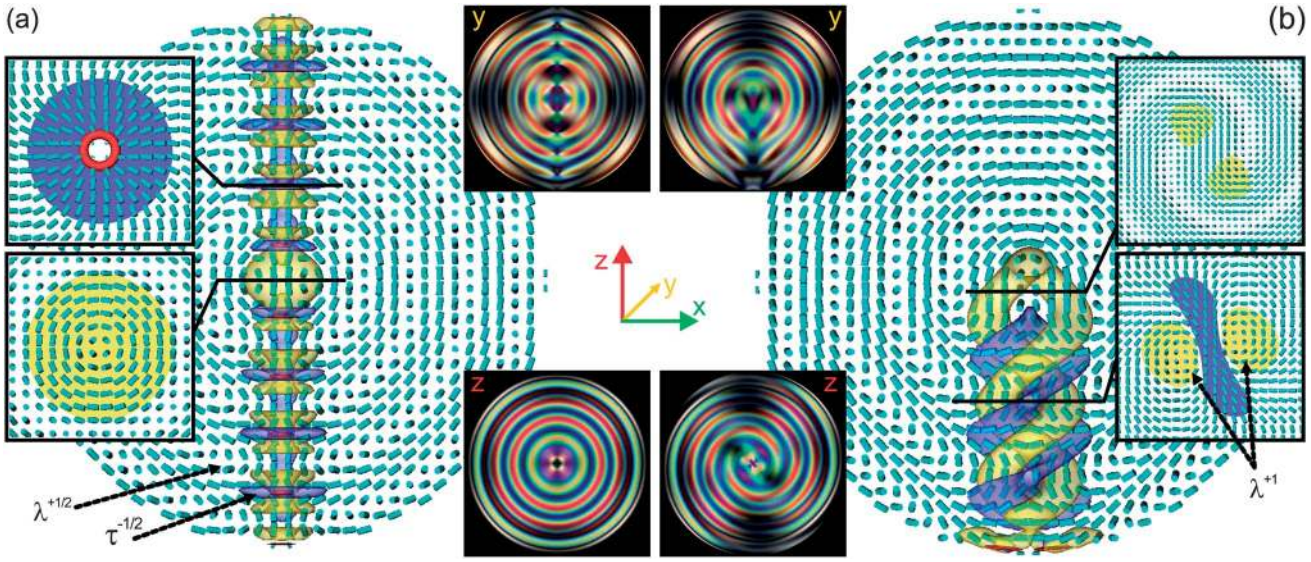

Fig. 2 Numerically calculated diametric spherical structure (DSS) and radial spherical structure (RSS) in chiral nematic droplets. Nematic order parameter is visualized as a red isosurface of $S = 0.48$ and the splay-bend parameter S_{SB} as blue ($S_{SB} \geq 0.0044$) and yellow isosurfaces ($S_{SB} \leq -0.0044$). The director field is visualized as light blue cylinders. (a) Diametrical spherical structure (DSS) for $N = 10$. Note red ring defects in the regions of the large positive splay-bend parameter (in blue). The insets show the director field at marked cross-sections and the polarization micrographs obtained for incident light along x and y directions. (b) Radial spherical structure (RSS) for $N = 10$. Note the double helicoidal shape of the yellow isosurface ($S_{SB} \leq -0.0044$) of splay-bend parameter. The insets show the director at marked cross-sections and polarization micrographs for light along y and z axes.

$$\begin{aligned} \boldsymbol{n} &= (\sin\phi\sin\theta, \cos\phi\sin\theta, \cos\theta), \\ \text{with } \phi &= \arctan\left(\frac{y}{x-d}\right) + \arctan\left(\frac{y}{x+d}\right), \theta \\ &= \arctan\left(\frac{2r_1r_2}{r_1+r_2}\right), \end{aligned} \tag{6}$$

where Φ and θ determine the director in-plane angle and the angle of escape, respectively. Distance from the effective center of the defect is equal to $r_{1,2} = \sqrt{(x \pm d)^2 + y^2}$. To model two +1 escaped disclination lines $d = 0.9$ is taken. Here, we should note that these '+1 escaped defects' actually correspond to cholesteric λ^{+1} defects that we see in numerical modeling. The escape needs to be modeled by a smooth functional of the escape angle that is nearly linearly dependent on the distance from the center of the disclination and asymptotically reaches $\pi/2$. The escape angle is predicted to decrease exponentially at asymptotically large distances.[37] Fig. 3a shows the director field and the splay-bend parameter of the structure extracted from the calculated RSS droplet (from Fig. 2b), reproduced by the Ansatz in eqn (6), whereas Fig. 3b shows the Frank-Pryce structure drawn by using effectively different Ansatz in eqn (6) with $d = 0$. The two profiles are clearly different if observing the region where the director escapes. The RSS droplet structure indicates that the director escapes in *two* separate regions corresponding to two λ^{+1} lines, whereas the Frank-Pryce model predicts one central region of escaped director. It is the chirality of the cholesteric competing with the formation of singular and non-singular cholesteric defect regions, which causes the two λ^{+1} disclination lines to wrap around one another forming the double helix structure (Fig. 3d).

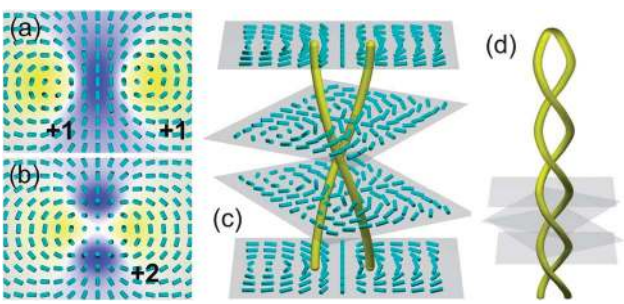

Fig. 3 Detailed view of a distorted cholesteric in the RSS structure and comparison to the Frank-Pryce model. Analytically constructed (a) two +1 escaped disclinations (actually corresponding to two λ^{+1} cholesteric disclinations) and (b) one +2 escaped disclination;[13] the splay-bend S_{SB} parameter is drawn in yellow and blue ($-0.044 < S_{SB} < 0.44$). Note that the core of the splay-bend parameter S_{SB} clearly differs between both defects. (c) Constructed director field on intersection planes with two λ^{+1} cholesteric disclinations rotating along the plane normal due to chirality. The center of λ^{+1} cholesteric disclination lines marked by the negative splay-bend parameter S_{SB} thus forms a double helix structure as seen in structures in Fig. 2b. (d) The two cores of +1 disclination lines forming a double helix structure and fusing together at the top (in the center of the droplet).

3.3 Bipolar structure

The third – *bipolar structure* (BS, Fig. 4a) – is cylindrically symmetric and is characterized by only two surface defects which are positioned diametrically. This structure gradually evolves from the bipolar structure in *non-chiral nematic* droplets when the chirality is effectively switched on and the cholesteric pitch becomes finite. The droplet is essentially formed from a λ^{+1} disclination line spanning diametrically along the cylindrical symmetry axis (z axis) of the droplet. The central region (around the z axis) is mostly uniformly aligned along the symmetry axis and is surrounded by several bent cholesteric layers in the form of

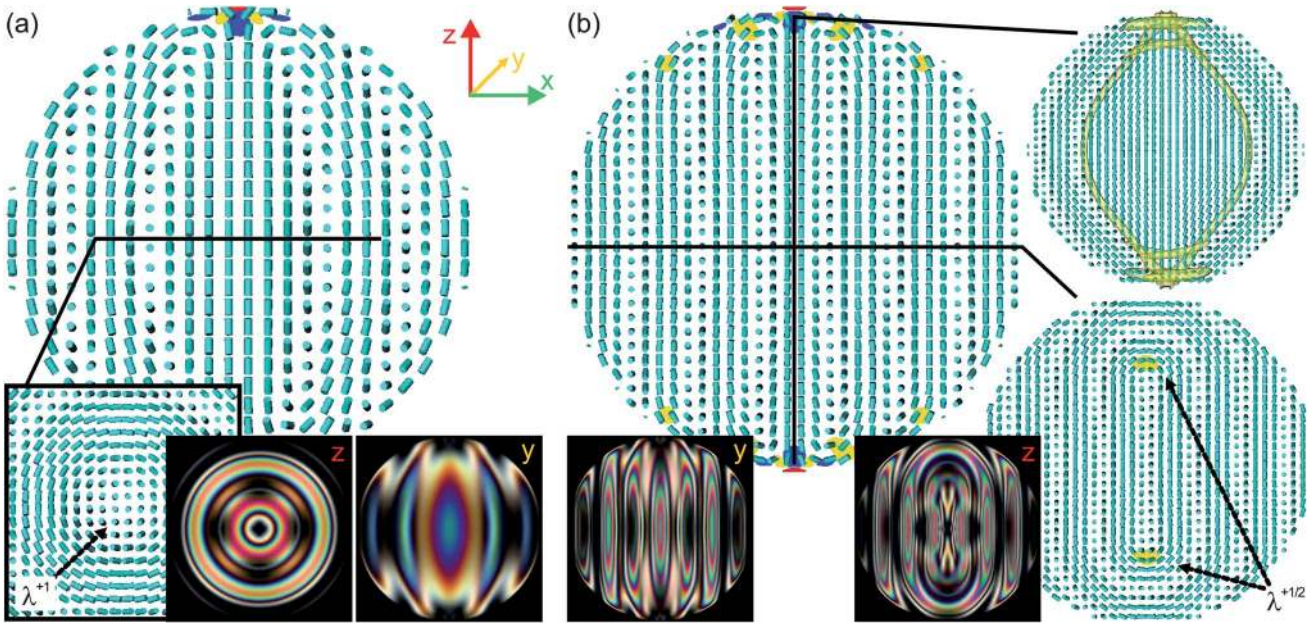

Fig. 4 (a) Bipolar structure (BS) with a diametrical λ^{+1} line for $N = 6$. Note the twofold axis that lies in the xy plane and the additional rotational symmetry around the z axis. (b) Planar bipolar structure (PBS) for $N = 8$. The director field in xz plane is mostly in layers as can be also seen in polarization micrographs. This structure has three twofold symmetry axes (x, y, and z). Note blue and yellow regions of the splay-bend parameter (blue at $S_{SB} = 0.0044$ and yellow at $S_{SB} = -0.0044$) and the differences between the two structures in polarization micrographs (lost symmetry in the z plane). Red isosurfaces represent defect regions with nematic degree of order $S = 0.48$.

distorted closed double twist tori (see left polarization micrograph in Fig. 4a). There is almost no noticeable divergence of splay or bend in the bulk, except small changes close to the two surface boojum defects. This structure is meta-stable up to $N \sim 6$ when it evolves into the stable radial spherical structure (RSS) by helicoidally winding the diametrical λ^{+1} line into the observed double helix structure (Fig. 2b and 3).

3.4 Planar bipolar structure

The *planar* bipolar structure (PBS, Fig. 4b) is closely related to the bipolar structure and also has two surface defects, positioned diametrically. The director field in the central region of the droplet forms cholesteric layers with layer normals in the x direction (see Fig. 4b and top right inset); however, near the surface the layers are deformed to satisfy the strong planar surface anchoring. This twisting, mostly near the surface, results in the splitting of the λ^{+1} line characteristic for the BS structure, into two $\lambda^{+1/2}$ lines observed now in the PBS structure. The two $\lambda^{+1/2}$ cholesteric disclinations are visualized well by the splay-bend parameter (in yellow) in Fig. 4b. Due to this splitting, the PBS structure is not fully rotationally symmetric as is the bipolar structure, but has only three twofold symmetry axes (axes x, y, and z). This broken symmetry results in non-spherically symmetric cholesteric layers (see bottom inset in Fig. 4b).

3.5 Lyre and Yeti structures

The other two structures found (see Fig. 5) are highly meta-stable and of bipolar type with only two surface defects positioned diametrically along the z axis. They both result from the χ^{+1} line[13,34] evolving into rings of $\lambda^{\pm 1/2}$ lines and have a double twist cylinder along the z-axis but differ in the symmetry of the nematic director field: the Yeti structure has higher symmetry due its additional two-fold symmetry along the arbitrary symmetry axis in the xy plane. However, contrary to the DSS structure (with $\tau^{-1/2}$ rings), in Lyre and Yeti structures the cholesteric disclinations in the form of rings are non-singular, as can be seen in Fig. 5.

The director field and the polarization micrograph of the *Lyre structure* (see Fig. 5a) resemble the shape of the lyre instrument. The Lyre structure is rotationally symmetric around the z axis. This structure is obtained by using Ansatz in eqn (4) and by choosing an appropriate N value (N has to be approximately even) such that the xy symmetry plane in the Ansatz vanishes. Only then such effective transformation of the χ^{+1} disclination line into $\lambda^{+1/2}$, $\lambda^{-1/2}$, and one λ^{+1} cholesteric disclination rings is observed, which are non-singular in the nematic director.

The Yeti structure (Fig. 5b) has also two diametrically positioned boojums and is related to the Lyre structure, but is obtained with approximately odd N in eqn (4). Thus, this structure has higher symmetry: a full rotational axis z as well as two-fold rotational axes in the xy plane. In the Yeti structure, the χ^{+1} line transforms into the central ring of λ^{+1} line, which is accompanied by additional $\lambda^{+1/2}$ and $\lambda^{-1/2}$cholesteric disclination rings. Here only the central λ^{+1} ring resembles the predicted toroidal spherulite structure.[24]

4 Stability of the structures

Fig. 6 shows the stability of the six structures in cholesteric droplets, as obtained by calculating the total free energy of each structure for a different pitch to size ratio $N = 4R/p_0$, and presenting the differences. Due to the high energy differences

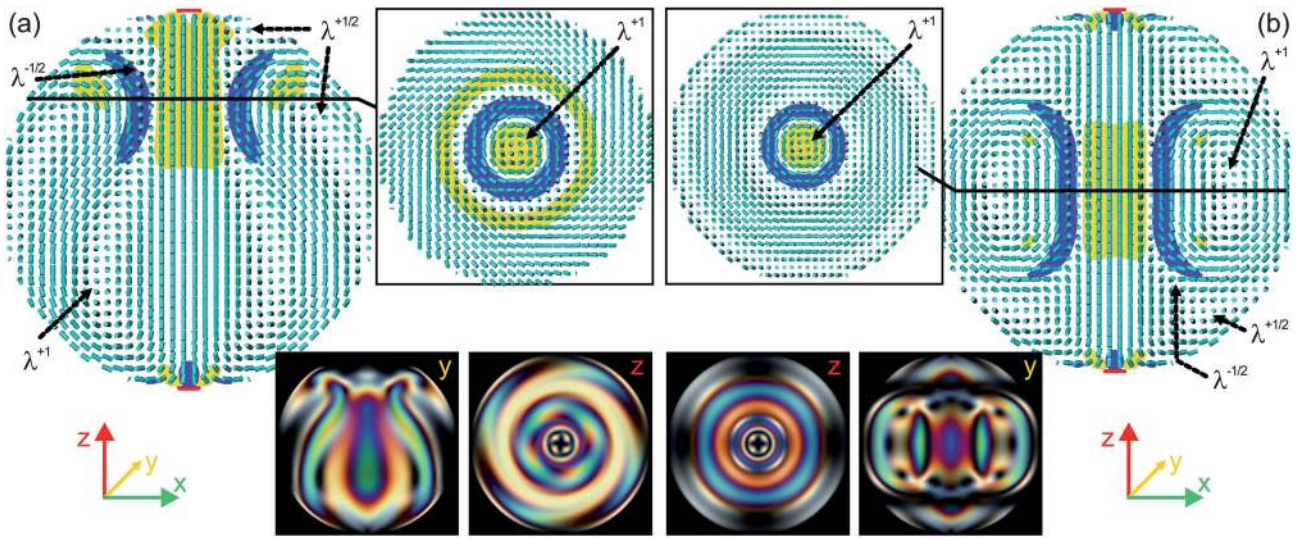

Fig. 5 (a) Lyre structure (LS, $N = 4$). Diametrical λ^{+1} line (see inset) with $\lambda^{+1/2}$, $\lambda^{-1/2}$, and λ^{+1} cholesteric disclination rings. The structure is only rotational symmetric around the z axis. (b) Yeti structure (YS, $N = 5$). Note also here the diametrical λ^{+1} line (see inset) and $\lambda^{+1/2}$, $\lambda^{-1/2}$, and λ^{+1} cholesteric disclination rings. Apart from the cylindrical rotational symmetry (z axis), this structure has also two-fold symmetry axes in the xy plane. Regions with reduced nematic degree of order are shown in red (isosurface of $S = 0.48$), whereas blue and yellow regions show the splay-bend parameter (at $S_{SB} = \pm 0.0044$).

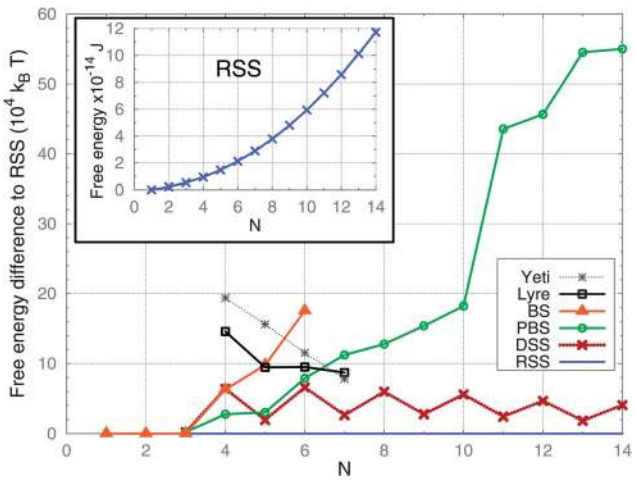

Fig. 6 Stability of the structures in cholesteric droplets. Free energy differences relative to the stable radial spherical structure (RSS) are calculated for: diametrical structure (DSS, in red crosses), planar bipolar structure (PBS, in green circles), bipolar structure (BS, orange triangles), Lyre structure (LS, in black squares), and Yeti structure (YS, in gray stars). Note the emergence of only one structure for a large pitch ($N \lesssim 3$) – the bipolar structure. Also, note the oscillation of the free energy difference for DSS for odd and even N. The Lyre and Yeti structures have much higher free energy than the other structures. Inset shows the total free energy for the RSS structure for varying N (*i.e.* varying the cholesteric pitch at fixed droplet size).

between the structures (of the order of $\sim 10^4\ k_B T$) the thermal fluctuations are not expected to provoke the transitions between the structures. We find the radial spherical structure to be the stable structure for spherical droplets with $N > 3$, which is also in good agreement with experiments.[1,21,24] At a chosen droplet size, the free energy difference between RSS and DSS structure decreases with increasing N (shorter pitch). However, for larger droplets the RSS structure is also the most stable structure with the DSS structure having higher total free energy (*e.g.* 0.07% higher free energy for $R = 3$ μm and $N = 20$). Interestingly, the free energy difference between the DSS and RSS structures oscillates for even N or odd N (see Fig. 6). Indeed, this corresponds to the DSS structure always having an even number of $\tau^{-1/2}$ ring defects (see Fig. 2) either for odd N (favourable) or even N when it is frustrated.

For small N ($N \lesssim 4$), the stable structure is the bipolar structure (BS) with a diametrical λ^{+1} line. However, for larger N, the bipolar structure becomes metastable and for $N \sim 8$ eventually unstable, transforming in our numerical relaxation algorithm into the radial spherical structure *via* the effective helical winding of the λ^{+1} line. Also, in contrast, by reducing N the radial spherical structure transforms back into the bipolar structure *via* the effective unwinding of the disclination line and pushing the surface boojum defects apart into the diametrically opposite positions (at $N \lesssim 3.5$).

The planar bipolar structure (PBS) emerges energetically more favorable (but still metastable) than the DSS structure for $N \lesssim 6$, whereas for larger N it has the highest free energy. Moreover, for $N > 10$ the free energy difference becomes substantial and thus PBS is not expected to be observed in experiments (not even as metastable). Experimentally, the PBS structure is typically found in deformed (non-spherical) cholesteric droplets.[2]

Even though the Lyre and Yeti structures may be expected to have low free energy due to the absence of the singular defects, they are found to be highly metastable. In these structures, the deformation of cholesteric layers is spun over the whole volume of the droplet, which is strongly energetically penalized. The free energy difference of the Lyre and Yeti structures relative to the stable structure decreases upon reducing the pitch; however, they remain metastable until $N \sim 7$ when they evolve into the radial spherical structure.

5 Conclusions

Structures in spherical cholesteric droplets with degenerate planar anchoring are explored, using mesoscopic numerical modeling. Three known structures – radial spherical, diametrical spherical, and planar bipolar – are found in this full calculation indeed to have the known general director profile, but have strongly different defect regions. These defects turn out to be cholesteric λ and τ defects, rather than nematic singular +1 or +2 defect lines. Further, we find two new (metastable) structures: the Lyre structure and Yeti structure.

We show that the effective defect structure of the radial spherical structure is composed of two λ^{+1} disclinations forming an interesting double helix. This double helix is explored in more detail by analytically calculating the director fields and by the splay-bend parameter that agree well with the numerical calculations. The diametrical χ^{+1} disclination line is found to be unstable. Firstly, in the numerical relaxation, it evolves into the diametrical spherical structure (DSS) where instead of the χ^{+1} a $\tau^{-1/2}$ and $\lambda^{+1/2}$ ring defects compensate for the structure of cholesteric layers. Secondly, it can also evolve into the newly found Lyre and Yeti meta-stable structures where the diametrical χ^{+1} cholesteric disclination is replaced by non-singular λ cholesteric disclination rings.

For small droplet radius-to-pitch ratio ($N \lesssim 4$), the energetically most favourable structure is the bipolar structure with diametrical λ^{+1} disclination. For larger radius to pitch ratios ($N > 4$), the radial spherical structure is the stable structure with the lowest free energy, in agreement with experiments. The planar bipolar structure is found meta-stable for all N and the free energy difference relative to the stable structures increases with larger N. The evolution of structures in cholesteric droplets when changing the cholesteric pitch can be understood as gradually adding additional cholesteric layers to the structure. Experimentally, changing the pitch could be achieved by controlling the chirality *via* temperature, dopants, or illumination with laser light. Moreover, taking into account the differences in splay, bend, and twist elastic constants, which we did not consider here and are known to be particularly important in systems such as lyotropic LCs or in nematics close to N–Sm transitions, will certainly affect droplet structures and their stability.

The transitions between the observed stable and meta-stable structures could be driven by applying complex electric fields as targeted stimuli. This would offer a route towards interesting switchable states, effectively memorised in the droplet. For example, if one could form different structures by shining[3,35] or by spatially steering Gaussian beams,[38,39] the transition from stable radial spherical structure to meta-stable diametrical spherical structure or even Yeti structure could perhaps be triggered optically. Generally, any change in the structure modifies optical and photonic properties of the droplets, which could be used as a possible mechanism to envisage soft matter optic and photonic elements in all-photonics circuits.

Acknowledgements

The authors would like to thank Oleg D. Lavrentovich, Randall D. Kamien, Hajime Tanaka, and Simon Čopar for valuable discussions and comments on the manuscript. The authors acknowledge financial support from ARRS program P1-0099. M.R. acknowledges EU MC Program FREEFLUID.

References

1 M. Humar and I. Muševič, *Opt. Express*, 2010, **18**, 26995.
2 D. J. Gardiner, S. M. Morris, P. J. W. Hands, C. Mowatt, R. Rutledge, T. D. Wilkinson and H. J. Coles, *Opt. Express*, 2011, **19**, 2432.
3 I. I. Smalyukh, Y. Lansac, N. A. Clark and R. P. Trivedi, *Nat. Mater.*, 2010, **9**, 139.
4 H. F. Gleeson, T. A. Wood and M. Dickinson, *Philos. Trans. R. Soc., A*, 2006, **364**, 2789.
5 Y. Yang, P. D. Brimicombe, N. W. Roberts, M. R. Dickinson, M. Osipov and H. F. Gleeson, *Opt. Express*, 2008, **16**, 6877.
6 W. Cao, A. Muñoz, P. Palffy-Muhoray and B. Taheri, *Nat. Mater.*, 2002, **1**, 111.
7 L. M. Blinov, G. Cipparrone, A. Mazzulla, P. Pagliusi and V. V. Lazarev, *J. Appl. Phys.*, 2007, **101**, 053104.
8 M. V. Kurik and O. D. Lavrentovich, *Pis'ma Zh. Eksp. Teor. Fiz.*, 1982, **35**, 263.
9 K. Tang, M. M. Green, K. S. Cheon, J. V. Selinger and B. A. Garetz, *J. Am. Chem. Soc.*, 2003, **125**, 7313.
10 S.-Y. T. Tzeng, C.-N. Chen and Y. Tzeng, *Liq. Cryst.*, 2010, **37**, 1221.
11 C. Ruslim and K. Ichimura, *J. Phys. Chem. B*, 2000, **104**, 6529.
12 M. Kleman and O. D. Lavrentovich, *Soft Matter Physics: An Introduction*, Springer-Verlag, 2001.
13 P. G. de Gennes and J. Prost, *The Physics of Liquid Crystals*, Oxford Science Publications, 2nd edn, 1993.
14 C. B. Stanley, H. Hong and H. H. Strey, *Biophys. J.*, 2005, **89**, 2552.
15 P. J. W. Hands, D. J. Gardiner, S. M. Morris, C. Mowatt, T. D. Wilkinson and H. J. Coles, *Appl. Phys. Lett.*, 2011, **98**, 141102.
16 G. P. Alexander, B. G. Chen, E. A. Matsumoto and R. D. Kamien, *Rev. Mod. Phys.*, 2012, **84**, 497–514.
17 S. Chandrasekhar, *Liquid Crystals*, Cambridge University Press, 2nd edn, 1993.
18 M. Kleman and J. Friedel, *J. Phys. (Paris), Colloq.*, 1969, **30**, C4–C43.
19 Y. Bouligand and M. Kleman, *J. Phys. (Paris)*, 1970, **31**, 1041.
20 M. V. Kurik and O. D. Lavrentovich, *Mol. Cryst. Liq. Cryst., Lett. Sect.*, 1982, **72**, 239.
21 F. Xu and P. P. Crooker, *Phys. Rev. E: Stat. Phys., Plasmas, Fluids, Relat. Interdiscip. Top.*, 1997, **56**, 6853.
22 J. Bezić and S. Žumer, *Liq. Cryst.*, 1992, **11**, 593.
23 J. Bajc, J. Bezić and S. Žumer, *Phys. Rev. E: Stat. Phys., Plasmas, Fluids, Relat. Interdiscip. Top.*, 1995, **51**, 2176.
24 Y. Bouligand and F. Livolant, *J. Phys.*, 1984, **45**, 1899.
25 C. Robinson, J. C. Ward and R. B. Beevers, *Discuss. Faraday Soc.*, 1958, **25**, 29.
26 M. V. Kurik and O. D. Lavrentovich, *JETP Lett.*, 1982, **35**, 444.
27 M. Ravnik, G. P. Alexander, J. M. Yeomans and S. Žumer, *Faraday Discuss.*, 2010, **144**, 159.
28 J.-B. Fournier and P. Galatola, *Europhys. Lett.*, 2005, **72**, 403.
29 M. Ravnik and S. Žumer, *Liq. Cryst.*, 2009, **49**, 1201.
30 S. Čopar, T. Porenta and S. Žumer, *Phys. Rev. E: Stat., Nonlinear, Soft Matter Phys.*, 2011, **84**, 051702.
31 R. Ondris-Crawford, E. P. Boyko, B. G. Wagner, J. H. Erdmann, S. Žumer and J. W. Doane, *J. Appl. Phys.*, 1991, **69**, 6480.
32 M. K. McCamley, G. P. Crawford, M. Ravnik, S. Žumer, A. W. Artenstein and S. M. Opal, *Appl. Phys. Lett.*, 2007, **91**, 141916.
33 M. Kleman, *Points, Lines and Walls*, John Wiley & Sons, 1983.
34 M. V. Kurik and O. D. Lavrentovich, *Sov. Phys. Usp.*, 1988, **31**, 196.
35 T. Porenta, M. Ravnik and S. Žumer, *Soft Matter*, 2012, **8**, 1865.
36 H.-S. Kitzerov and P. P. Crooker, *Liq. Cryst.*, 1993, **13**, 31.
37 A. Bogdanov, *JETP Lett.*, 1995, **62**, 251.
38 P. J. Ackerman, Z. Qi and I. I. Smalyukh, *Phys. Rev. E: Stat., Nonlinear, Soft Matter Phys.*, 2012, **86**, 021703.
39 P. J. Ackerman, Z. Qi, Y. Lin, C. W. Twombly, M. J. Laviada, Y. Lansac and I. I. Smalyukh, *Sci. Rep.*, 2012, **2**, 414.

